13th International Symposium on Particle Image Velocimetry – ISPIV 2019
Munich, Germany, July 22-24, 2019

PIV measurements of the flow around an aero-engine intake inside an icing wind tunnel.

Juan S. Velandia[1*], **Stephan E. Bansmer**[1]

[1] Technische Universität Braunschweig, Institute of Fluid Mechanics, Braunschweig, Germany

[*] j.velandia-rodriguez@tu-braunschweig.de

Abstract

Aero-engine intakes are sensitive components where the accumulation of ice can modify the inflow of the engine and alter its performance. To study the airflow in this case, the ice accretion is generated and studied in an icing wind tunnel environment. Non intrusive measurement techniques are needed to assess the velocity field around the inlet. Wind tunnel contamination due to foreign particles can be a major issue for this kind of facilities and needs to be avoided. We show PIV results using water droplets as seeding material and applying two correction methods accounting for the droplet's drag to improve the velocity estimations. Our results suggest that correcting the air velocity calculated from the particle trajectory using the Stokes drag law increases the accuracy of the measurements.

1 Introduction

New generation aero-engine intakes are characterized by shorter lips and a higher by-pass ratio. These features increase the complexity of the flow at the intake, particularly when subjected to off-design conditions like high incidence. It has been shown that changes in the shape (Coschignano et al., 2019) or roughness (Coles and Babinsky, 2019) on this element can deteriorate the air flow at the fan stage of the engine. Some of the events inducing such changes include insect contamination and ice accretion.

Ice accretion occurs when an aircraft flies across clouds where icing conditions exist. In these clouds, water droplets below freezing temperatures, named supercooled droplets, hit any exposed surface of the airplane and freeze. The size of the droplets and the amount of water on the cloud are commonly described by the median value diameter (MVD, in μm) and the liquid water content (LWC , in gm^{-3}) of the cloud. These two parameters, the ambient temperature, the flight velocity and the size of the body being hit by the water droplets define the shape and characteristics of the accretion.

Mainly due to high costs and risks in real flight tests, icing wind tunnels (IWT) appear as a great opportunity to study such events. This kind of tunnels has the capability to chill the air and to produce different cloud conditions by injecting water droplets into the flow. A simplified aero-engine intake was mounted in the test section of the Braunschweig icing wind tunnel to run icing tests on it. The simplified profile, as well as the test section of the wind tunnel, were adapted to replicate the flow of the reference case described by Coschignano et al. (2019).

Particle image velocimetry (PIV) was used in the region around the leading edge of an aero-engine intake at incidence. Conducting these measurements in an IWT is challenging because, apart from regular requirements of the technique, the seeding selection presents additional difficulties. The selection of seeding has to consider that no contamination will remain in the tunnel after the measurements are done. To avoid the inclusion of foreign particles in the tunnel, water droplets can be used as seeding particles for PIV measurements, as shown by De Gregorio (2008). Nevertheless, it has to be considered that the size of the particles seeded is larger than the one recommended for PIV measurements (Raffel et al., 2018). Since larger particles have difficulties to follow high velocity gradients, a correction is applied to the measured velocities to reconstruct the air velocity field.

Different corrections have been applied to particle velocimetry methods. In some of these methods, the particle's acceleration is assumed to be affected only by the drag force. Flows with shock waves appear as a typical high velocity gradient flow where these corrections have been done. A correction based on the Stokes drag law was proposed by Koike et al. (2007) to increase the clarity of shock waves in PIV measurements.

Another drag correction is adopted by Boiko et al. (2013) considering non-Stokes particles and showing that this kind of corrections can be applied to flows with discontinuities, like the ones presenting shock waves. These methods approximate particle acceleration by calculating spatial gradients of velocities measured by optical means. Such estimations are also common when deriving pressure values from PIV measurements (van Oudheusden, 2013).

We present the results of PIV measurements on an aero-engine intake without ice at incidence with water droplets as seeding particles in an icing wind tunnel. The results are compared to numerical simulations, which are considered as the reference velocity field to be measured. The vector fields obtained by the measurements are corrected by two different drag laws. It is observed that, for the studied case, the Stokes drag law seems to be sufficiently accurate to correct the velocity field. First, this paper will present the set up used for the PIV measurements. Second, a brief description of the method to correct the air velocity is stated, where the velocity is calculated from the droplet trajectory. Third, results of the measurements and the corrections applied to the particle trajectories are shown. The results are promising and are to be considered when doing measurements on iced test objects.

2 Experimental set up

2.1 Icing wind tunnel

The tests were run in the Braunschweig Icing Wind Tunnel (IWT). A scheme of the IWT can be seen in fig. 1. The IWT is a closed loop tunnel with icing capabilities. The flow is driven by a fan located in the upper section of the tunnel. The heat exchanger is operated by a cooling plant and chills the air flow to produce icing temperatures in the test section (as low as $-20\ ^{\circ}C$). Cooled air goes through the screens and reaches the spray system in the settling chamber of the tunnel. This system is composed by an array of 5×6 atomizers. The atomizers generate water droplets that are supercooled by the chilled air and form an icing cloud that enters the test section of the tunnel ($0.5\ m \times 0.5\ m \times 1.5\ m$) at a velocity up to 40 m/s. The size and the amount of the droplets generated are characterized by the Median Value Diameter (MVD, measured in μm) of the droplets distribution and the Liquid Water Content (LWC, measured in gm^{-3}) of the cloud. The droplets size can be varied in a range between 8 μm and 65 μm and the LWC can be set to values up to 3 gm^{-3}. More details on the IWT can be consulted in Bansmer et al. (2018).

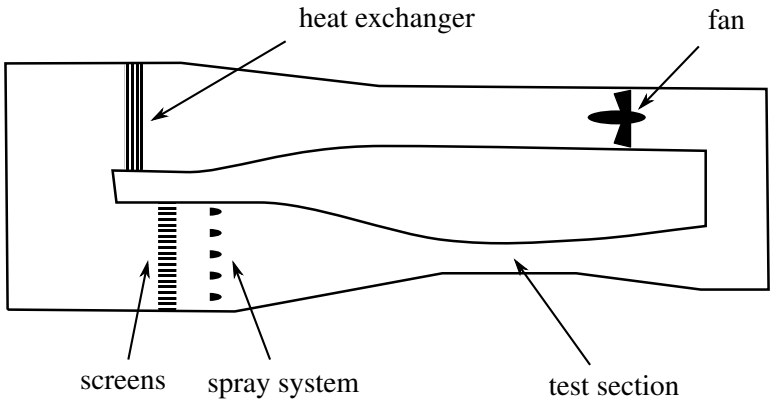

Figure 1: Icing wind tunnel scheme

2.2 Test section and PIV set up

The test section of the IWT was adapted to the replicate key features of the flow found in the reference case by Coschignano et al. (2019). The profile is inspired in the lower section of a nacelle case over the intake of an aero-engine. Two deflection elements were included, as can be seen in Fig. 2. The purpose of these elements is to deviate the flow from an horizontal path and to locate the stagnation point to match the reference case.

One drawback of this design is that the deflectors constrain the visual access to the test section from the top and the bottom. This leads to an elaborated PIV setup because the laser sheet illuminating the seeding

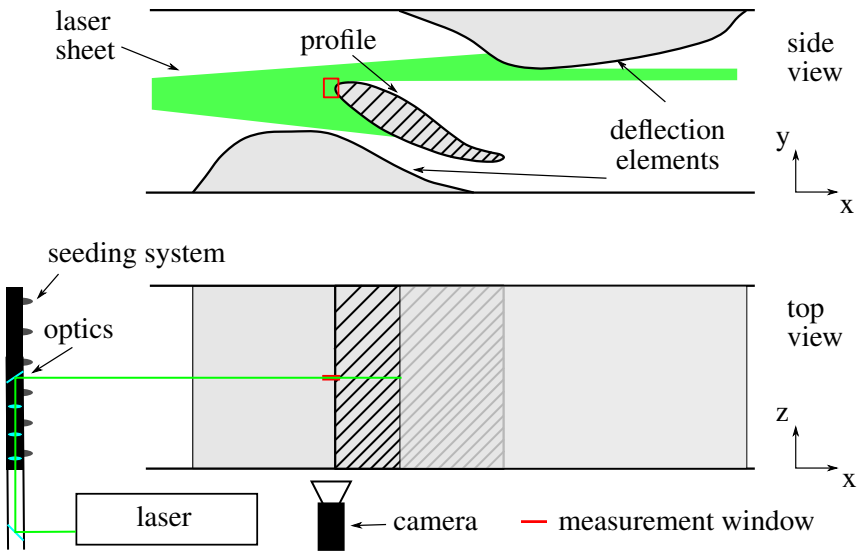

Figure 2: Side and top view of the test section set up scheme.

has to hit the profile leading edge from the settling chamber of the tunnel, as shown in Fig. 2. The PIV setup is composed by a laser located next to the wind tunnel, a set of lenses and mirrors, located in the settling chamber, above the spray system, and a camera located next to the test section. A Nano T PIV pulsed Nd:YAG laser from the company Litron Lasers was used to create the laser sheet in the measurement window. The set of optics is composed by a planoconcave, a planoconvex and a cylindrical lens. These elements where mounted on the spray system. The distance between the last mirror and the measurements window is 4.2 m. The width of the laser sheet was 5 mm. The camera used is a sensicam qe with a resolution of 1376 $\times$ 1040 pixels. An objective Nikkor AF D 60/2,8mm was employed to set the focus on the laser sheet at 0.23 m of the camera.

The images for the PIV where taken in a measurement window of 50 $mm \times 35$ mm. The time between two laser shots and the image capture was set to 6.2 μs. Up to 2000 images were recorded for each of the seeding used; nevertheless, because of the non homogeneous spatial distribution of seeding, only 300-400 double frames were used for further analysis. All images were masked to ignore the reflections produced by the profile surface during the postprocessing. To produce velocity fields, the cross-correlation method was used. A multi-pass approach was set with round interrogation windows from 512×512 pixels to 32×32 pixels. The acquisition of images and postprocessing was done with the software DaVis 8.3 from LaVision.

2.3 Water droplets as seeding for PIV

As mentioned above, seeding particles for PIV purposes in an icing wind tunnel have to be carefully chosen. The major concern of injecting any foreign particle in the tunnel is the risk of leaving traces once the PIV tests are finished. For icing purposes, any solid particle left in the tunnel is a potential nucleation point promoting a change of phase for supercooled water droplets. Any kind of oil or Di-Ethyl-Hexyl-Sebacat (DEHS, usually used for PIV measurements) sediments in the tunnel needs to be avoided.

Making use of the installed capacity to inject water droplets in the settling chamber of the IWT, the airflow will be seeded with such droplets for the PIV measurements. This approach was conducted in another facility and proved to be successful by (De Gregorio, 2008). Four different atomizers sets were used during these tests, producing cloud conditions with MVD values of 10 μm, 20 μm, 35 μm, and 55μm. Compared to common PIV seeding particles, the water droplets used present several differences. First, the particles are several times larger than the oil particles used typically for such techniques ($d < 4$ μm). Second, the particle size distribution generated by the atomizers in the IWT is broad, as can be seen in Fig. 3 for the $MVD \approx 10$ μm case. The uncertainty regarding the size of the particles is therefore large. Small particles might follow the airflow, but the larger ones, also seeded in the flow at the same time, might distort the measurements.

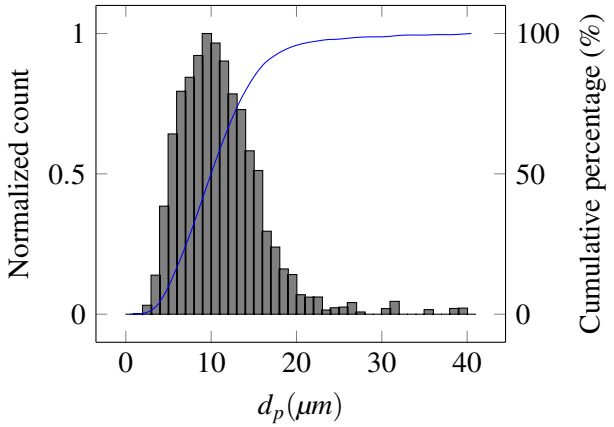

Figure 3: Water droplet distribution for $MVD \approx 10\mu m$.

3 Air velocity calculation from water droplet trajectory

The particles seeded to the flow are so large that, depending on the characteristics of the flow, the measured velocity ($\vec{u_p}$) can differ from the air velocity ($\vec{u_f}$). A correction to the particle velocity is proposed, considering that particles are accelerated by the flow they are immersed in. A force balance in a single droplet, considering only the aerodynamic drag, gives:

$$\frac{d\vec{u_p}}{dt} = F_D(\vec{u_f} - \vec{u_p}), \tag{1}$$

where F_D is a factor explained later in this section. Nevertheless, PIV data is generated by two frames separated by a known time. Two locations are not sufficient to estimate the acceleration of the particle. Applying the rule of chain, the temporal derivative can be estimated as a spatial derivative, as follows:

$$u_p\frac{\partial u_p}{\partial x} + v_p\frac{\partial u_p}{\partial y} = F_D(u_f - u_p), \tag{2}$$

$$u_p\frac{\partial v_p}{\partial x} + v_p\frac{\partial v_p}{\partial y} = F_D(v_f - v_p), \tag{3}$$

where u_i and v_i are the horizontal and vertical components of the velocity vector $\vec{u_i}$ and i takes the value of f to describe the air flow velocity and the value of p to describe the particle velocity. The local derivatives of the particle velocity can be estimated from the velocity fields obtained from the PIV results. Thus, the corrected fluid velocities, u_{f_x} and u_{f_y}, can be calculated by:

$$u_f = u_p + \frac{1}{F_D}(u_p\frac{\partial u_p}{\partial x} + v_p\frac{\partial u_p}{\partial y}), \tag{4}$$

$$v_f = v_p + \frac{1}{F_D}(u_p\frac{\partial v_p}{\partial x} + v_p\frac{\partial v_p}{\partial y}). \tag{5}$$

Two different approaches can be taken to calculate the value of F_D. Assuming that the flow around the particle is a Stokes flow, it can be inferred that the drag depends only on the particle diameter (d_p), air viscosity (μ_f) and particle density (ρ_p). In this case, the value of F_D is named $F_{D_{St}}$ (see Eq. 6). If the flow around the particle does not comply this condition, which is usually the case for larger particles, the drag coefficient and the Reynolds number of the particle take part into the estimation of F_D and we name it $F_{D_{Re_p}}$ (see Eq. 7).

$$F_{D_{St}} = \frac{18\mu_f}{\rho_p d_p^2} \tag{6}$$

$$F_{D_{Re_p}} = F_{D_{St}} \times \frac{C_d Re_p}{24} \tag{7}$$

The value of the drag coefficient (C_d) depends on the Reynolds number and are calculated after Morsi and Alexander (1972). Both corrections are applied to the PIV results and shown in the results section. The air velocity calculated from the corrections applying $F_{D_{St}}$ is named $\vec{u}_{St_{d_p}}$ and the one applying $F_{D_{Re_p}}$, $\vec{u}_{Re_{d_p}}$.

4 Results

The Fig. 4 shows the results for the different measured cases. An example of the images captured can be observed in the first row of the figures. A high concentration of particles is present above the leading edge, which will be addressed later.. The second row of the image shows the averaged velocity field for the four different measurements. No relevant differences can be observed between the different particles' diameter. The stagnation region of the profile is not well defined and appears as a broad area instead of a well defined region.

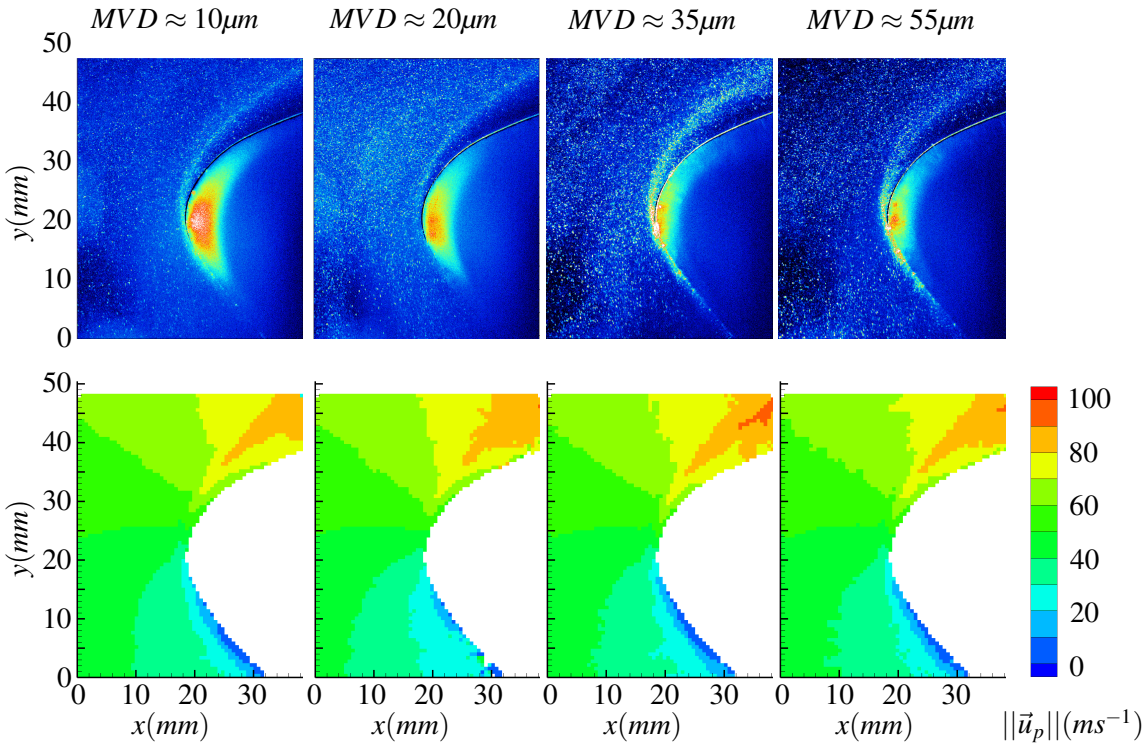

Figure 4: PIV results for different water droplet size.

In order to have a reference for comparing the PIV results with, a numerical simulation of the tunnel setup was conducted. A 2D simulation of the setup shown in Fig. 2 was performed. The simulation was conducted solving the Reynolds-averaged Navies-Stokes (RANS) equations. All the walls on the setup were considered adiabatic and the turbulence was modelled using the SST $k-\omega$ model. Water droplets were injected and their trajectory was calculated using the discrete phase model. The droplets injected had a MVD of $\approx 10\mu m$. Fig. 5 shows the comparison between the PIV measurements and the simulated droplets trajectories. The high concentration of particles mentioned before can be explained by the accumulation of particles in this region. The particles seem not to be able to follow an important change in the direction of the flow attached to the profile. The acceleration of the flow in this region seems to be too large for the particles to follow it. The path they are able to follow corresponds to the region highly illuminated in the PIV measurements. Even if there is a lack of particles near to the profile, the trajectory of most of the particles agrees with the simulated ones. Reducing the diameter of the particles might help to describe better this

region, the particles' trajectories are expected to follow better the flow and fill the empty region observed in Fig. 5.

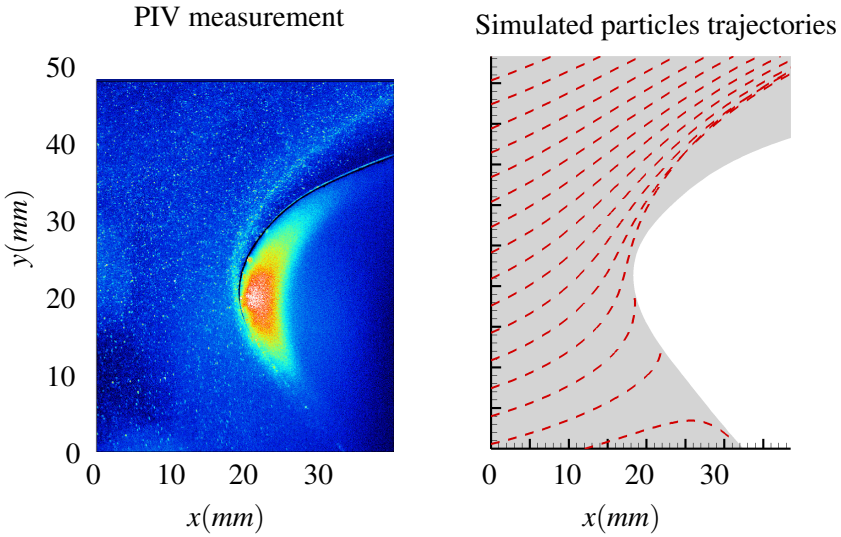

Figure 5: PIV recorded frame and particles trajectories from simulation for $MVD \approx 10\mu m$

The velocity contour for the simulated flow, $||\vec{u}_f||$, is shown in Fig. 6, as "Simulation". Since the variation of the diameter does not seem to have a large influence on the results, only the $MVD \approx 10\ \mu m$ will be analyzed from now on. The velocity measured by PIV is lower than the one predicted by the simulation. Air streamlines and particle trajectories are also compared on the right of the figure. It can be seen that the water droplets enter the measurement window in a flatter angle compared to the air flow and fail to follow the flow close to the profile.

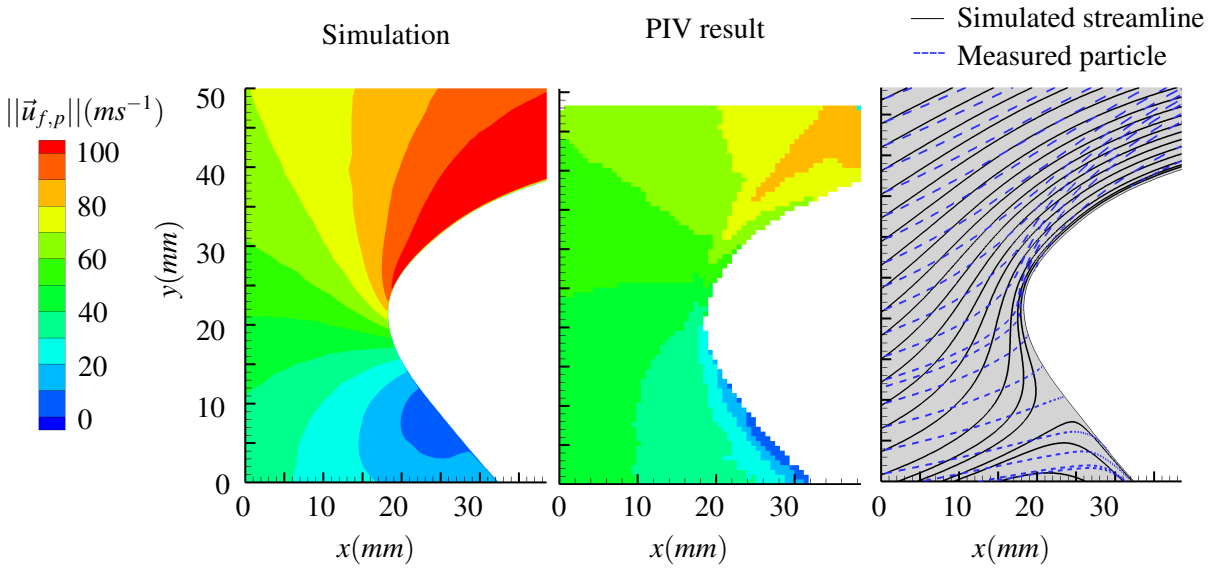

Figure 6: Air streamline (from simulation) and water droplet trajectory comparison for $MVD \approx 10\mu m$

The correction proposed to calculate the air velocity in the previous section is applied to the particle trajectories shown in Fig. 6. The corrected streamlines, shown in Fig.7, have a better agreement to the flow in the region far from the profile. The angle of entry of the corrected velocity, namely the corrected streamlines, is closer to the one of the airflow. A large accumulation of streamlines appears in the region

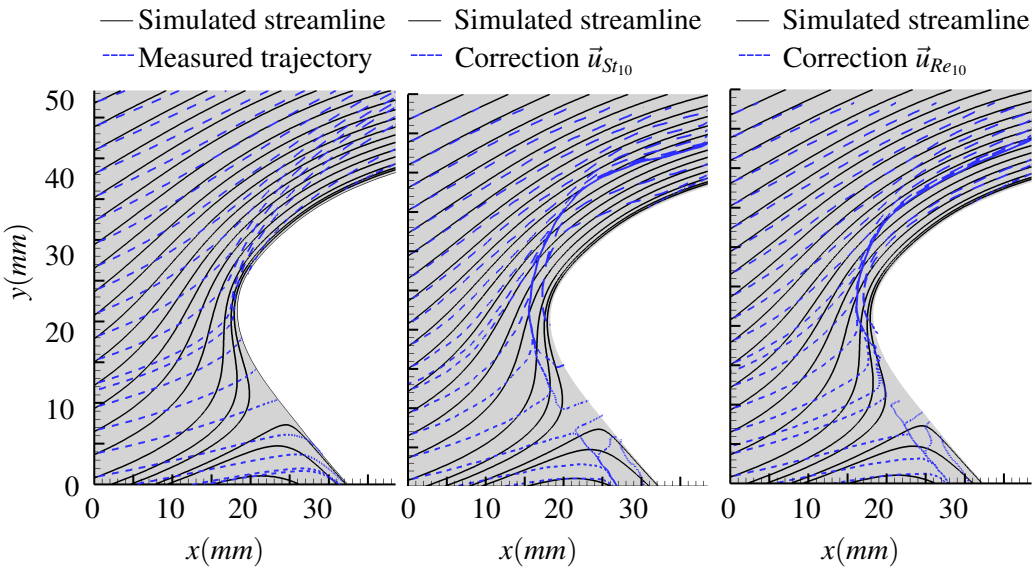

Figure 7: Reference streamline and streamline reconstruction for $MVD \approx 10\mu m$.

where the particles have a higher density in the images taken, explained in Fig. 5. Some problems appear close to the profile, where the corrected streamlines seem to leave the profile and join the high density region, which does not represent the real behaviour of the flow. This problems can arise because the gradients in the region close to the profile are larger than in the potential flow region. Since the correction terms depend on the gradients of the measurements, inaccuracies on the measurements can explain such problems. Both corrections, considering the particles as immersed in a Stokes flow and calculating their drag as a function of Re_{d_p}, show a better agreement to the flow in the potential region but lack of accuracy close to the profile. No big difference can be appreciated up to this point in both correction methods. To compare both correction methods, values of magnitude ($||\vec{u}_i||$) and direction (α_i) of the velocity vectors were extracted for two planes at $x = 10\ mm$ and $x = 18\ mm$ and are shown in Fig. 8 and Fig. 9 respectively.

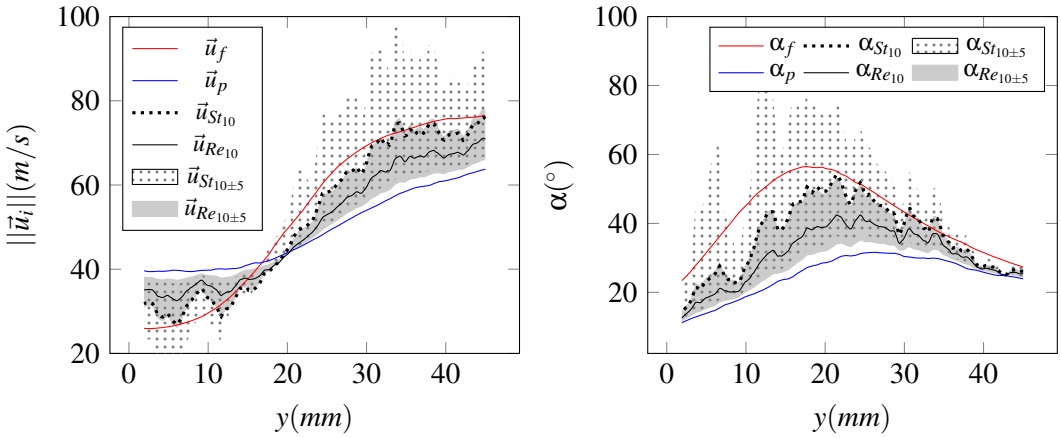

Figure 8: Velocity magnitude and direction correction for the line $x = 10mm$.

Considering that the reference velocity is given by the numerical simulations, the corrections implemented should shift the velocity estimated by the PIV measurements ($\vec{u}_p$) closer to the reference one ($\vec{u}_f$). The changes in velocity magnitude shown in Fig. 8 prove that both methods have this effect. For $0\ mm < y < 20\ mm$, the correction decelerate the flow, while for $20\ mm < y < 45\ mm$ it increases the flow velocity. Surprisingly, the method assuming that the water droplets are considered as immersed in a Stokes flow (dotted line) seem to have a better agreement with the reference field. Both corrections show a rougher

velocity profile than the simulation or the measurements. This can be explained by the fact that the velocity gradient is calculated in a discrete way and inaccuracies on this operator are expected. A variation in the value of the droplet's diameter (d_p) was included in the corrected velocity by calculating the correction for $d_p + 5\ \mu m$ and $d_p - 5\ \mu m$ and coloring the area in-between. This variation, shown as $\vec{u}_{St_{10\pm5}}$ for the Stokes drag assumption and as $\vec{u}_{Re_{10\pm5}}$ for the other drag law in Fig. 8 and Fig. 9, has a larger influence in the correction considering the Stokes drag. Even if this method seems to be more accurate that the other drag law applied, it is more sensitive to the value of the droplet's diameter used. This confirms that the diameter of particles is of paramount importance for applying this correction appropriately. In any case, the corrected velocity has a fairly good agreement with the reference.

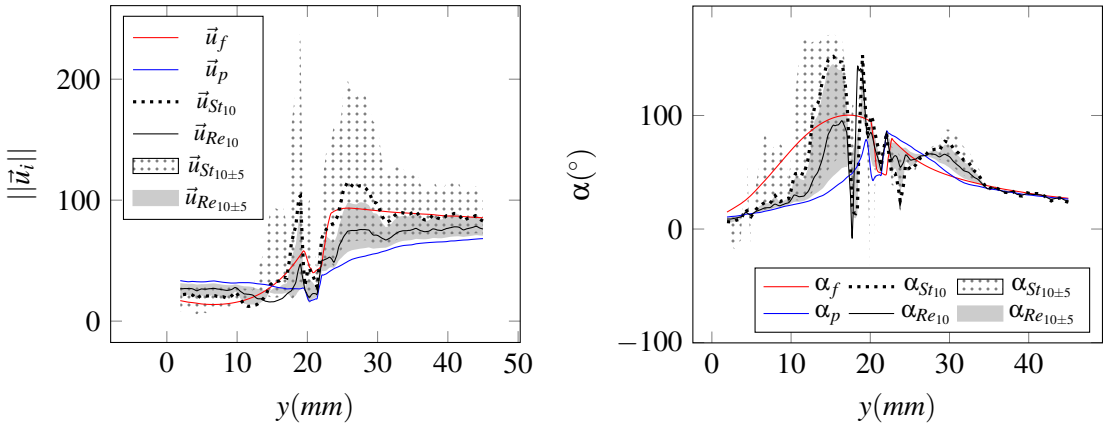

Figure 9: Velocity magnitude and direction correction for the line $x = 18mm$.

Fig. 9 shows the same comparison as the previous figure, but for a plane located at $x = 18\ mm$. This plane is closer to the profile and thus the changes in velocity are stronger. The same behaviour described for the previous figure can be seen in this case. The correction assuming that the droplets are in a Stokes flow agrees better with the reference velocity. Since the changes in velocity are stronger here, it can be seen that large velocity gradients weaken the effectiveness of the approach. $||\vec{u}_{St_{10}}||$, for example, fails to capture the acceleration of the flow at $y = 19\ mm$ and overpredicts it. More accurate measurement and gradient estimations would enhance the capability of both correction methods to match the reference field.

5 Conclusion

Water droplets were used as PIV seeding to measure the airflow around an aero-engine intake in an icing wind tunnel. Four different droplet sizes were used during the tests. No considerable differences were found in the results as the diameter of the droplets was changed. The stagnation point on the profile was not well assessed by the measurements and the droplets seem to have issues following the flow in the acceleration region over the profile.

The corrections proposed improves the prediction of the velocity in the regions further away from the profile. Both methods reduce the gap between the reference field and the one measured by PIV. Close to the profile, where stronger velocity gradients are present, both corrections fail to reconstruct the reference field. The approaches proposed are therefore very sensitive to velocity gradient estimations. The method in which particles are treated as being in a Stokes flow has a better agreement with the reference field, nevertheless, it is the more sensitive one to changes in the diameter of the particles when applying any correction.

In order to enhance the accuracy of the methods, a better estimation of the water droplets diameter has to be assessed. A higher resolution on the measurement windows could also lead to a more accurate estimation of the velocity gradients as well as to reducing the roughness of the corrected velocity profiles. To improve both estimations, other optical measurement techniques, such as shadowgraphy, could be conducted. Once the accuracy of the methods is improved, tests will be run on an iced geometry, where the presence of ice is expected to disturb the air flow considerably.

Acknowledgements

We thank the German Academic Exchange Service (DAAD grant no. 57214224) for supporting the first author and Denis Sotomayor Zarakhov for his help in the implementation of the correction methods.

References

Bansmer SE, Baumert A, Sattler S, Knop I, Leroy D, Schwarzenboeck A, Jurkat-Witschas T, Voigt C, Pervier H, and Esposito B (2018) Design, construction and commissioning of the braunschweig icing wind tunnel. *Atmospheric Measurement Techniques* 11:3221–3249

Boiko VM, Pivovarov AA, and Poplavski SV (2013) Measurement of gas velocity in a high-gradient flow, based on velocity of tracer particles. *Combustion, Explosion, and Shock Waves* 49:548–554

Coles C and Babinsky H (2019) The impact of roughness size on the shock-wave boundary-layer interaction on aero-engine intakes at incidence.. in *AIAA Scitech 2019 Forum*

Coschignano A, Babinsky H, Sheaf C, and Zamboni G (2019) Normal-shock/boundary-layer interactions in transonic intakes at high incidence. *AIAA Journal (Articles in Advance)* 0:1–14

De Gregorio F (2008) *Aerodynamic Performance Degradation Inducedby Ice Accretion.PIV Technique Assessment in Icing Wind Tunnel*. pages 395–417. Springer Berlin Heidelberg

Koike S, Takahashi H, Tanaka K, Hirota M, Takita K, and Masuya G (2007) Correction method for particle velocimetry data based on the stokes drag law. *AIAA Journal* 45:2770–2777

Morsi S and Alexander A (1972) An investigation of particle trajectories in two-phase flow systems. *Journal of Fluid Mechanics* 55:193208

Raffel M, Willert CE, Scarano F, Kähler CJ, Wereley ST, and Kompenhans J (2018) *Particle Image Velocimetry*. page 39. Springer. 3rd edition

van Oudheusden BW (2013) PIV-based pressure measurement. *Measurement Science and Technology* 24:032001